Optimization of Air-Gap Profile in Interior Permanent-Magnet Synchronous Motors for Torque Ripple Mitigation

Jingchen Liang, *Student Member, IEEE*, Amir Parsapour, Zhuo Yang, *Student Member, IEEE*, Carlos Caicedo-Narvaez, *Student Member, IEEE*, Mehdi Moallem, *Senior Member, IEEE*, and Babak Fahimi, *Fellow, IEEE*

***Abstract*— Interior permanent-magnet synchronous motors (IPMSMs) have been widely used due to their high-efficiency and high-power densities. Minimization of torque pulsation resulting in vibration and acoustic noise is one of the important design considerations for IPMSMs. In this paper, a grid on/off search method for the rotor profile is proposed to mitigate torque pulsation. Selection of the rotor profile is due to the fact that air gap is the most sensitive parameter in electric machines wherein changes in flux densities can cause substantial differences in the distribution of forces. A layer comprised 20 partitions with a 0.1 mm thickness and 3° wide grids have been introduced to the rotor surface for each pole, and the possible geometries have been analyzed using the finite-element method in ANSYS Maxwell. An optimal design was found that has the lowest torque ripple with a higher average torque compared to the original design. Genetic algorithm has also been applied to the method to automate the coupling between Maxwell and MATLAB, thereby saving the simulation time. Complete structural analysis has been done for both of the original and optimal designs to verify the superiority and feasibility of the proposed design.**

***Index Terms*— Air-gap optimization, genetic algorithm (GA), interior permanent-magnet synchronous motor (IPMSM), torque ripple.**

I. Introduction

INTERIOR permanent-magnet synchronous motors (IPMSMs) have broad applications in electric vehicles, home appliances, and robotics due to their high-power densities, high torque densities, and large speed ranges [1], [2]. Permanent magnets are buried inside the rotor, which leads to an unequal permeability for the d-axis and q-axis leading to magnetic saliency. Given the presence of reaction torque, caused by the magnetomotive force (MMF) of the stator and its interaction with permanent magnets, the torque of IPMSM is a combination of reaction and reluctance torques, which provides a higher torque density and wider speed range during field weakening compared to other conventional machines [3].

However, torque pulsation is one of the most important design considerations in IPMSMs, since it can cause unwanted byproducts such as vibrations and acoustic noise. Mitigation of torque pulsation has been studied by many scholars. There are mainly two categories of methods, namely, control techniques such as the current profiling method [4], [5], and the optimal design method. However, reducing torque pulsation based on power electronics and control method heavily depends on the accuracy of the power electronics circuits as well as the need for high-end microcontrollers to guarantee a timely execution of the control algorithm. This paper proposes a torque ripple minimization method from the design point of view. Many techniques have addressed this topic, such as rotor or stator skewing [6]–[8], magnet skewing and shape optimization [7], slot/pole number combinations [7], [9], [10], optimization of flux barrier such as asymmetric flux barriers [11], rotor shape optimization, such as Kiyoumarsi and Moallem [12], Kioumarsi *et al.* [13], and Yoon and Kwon [14] reported an optimal shape design obtained by drilling small circular holes in the rotor, and unequal air-gap length optimization [15]–[18].

The main purpose of air-gap profile optimization is to redistribute the flux density and force components on the rotor surface with a smoother profile while keeping the average air-gap flux and torque density constant. Therefore, in this paper, a grid on/off search method on the rotor surface is introduced to optimize the air-gap profile such that not only the torque pulsation is mitigated but also the average torque and overall performance of the motor are improved. Grid on/off search method is implemented by introducing a layer of partitions on the rotor surface; the material of each partition can be assigned as either air or iron, represented as "0" and "1" in the simulation process, which is similar to turning on and off switches in digital logic. Multiple simulations are executed, and their results are compared in order to search for an optimal combination of partitions to meet the optimization goal.

Furthermore, in order to reduce the simulation time, genetic algorithm (GA) is applied to this method. In the optimization process, software Maxwell has been coupled to MATLAB to automate the simulation process. Simulation results using the finite-element method (FEM) in ANSYS Maxwell as well as the structural analysis in ANSYS Workbench are presented for

Manuscript received July 31, 2018; revised November 21, 2018; accepted December 31, 2018. Date of publication January 21, 2019; date of current version March 19, 2019. *(Corresponding author: Jingchen Liang.)*

J. Liang, A. Parsapour, and C. Caicedo-Narvaez are with the Department of Electrical and Computer Engineering, The University of Texas at Dallas, Richardson, TX 75080 USA (e-mail: jxl146930@utdallas.edu).

Z. Yang is with the Department of Electrical and Computer Engineering, The University of Texas at Dallas, Richardson, TX 75080 USA.

M. Moallem is with the Department of Electrical and Computer Engineering, Isfahan University of Technology, Isfahan 841583111, Iran.

B. Fahimi is with the Department of Electrical and Computer Engineering, The University of Texas at Dallas, Richardson, TX 75080 USA.

Digital Object Identifier 10.1109/TTE.2019.2893734

both the original and optimal designs to validate the feasibility of the optimal design.

The remainder of this paper is organized as follows. Section II presents the analytical model for IPMSMs and the 2-D model constructed in ANSYS Maxwell for this design. Section III introduces the grid on/off search method and the GA applied thereto. Section IV presents the simulation results for both the original and the optimal designs. The structural analysis will be discussed in Section V.

II. IPMSM Model

In order to understand the influence of the air-gap profile on torque pulsations in IPMSMs, it is necessary to construct the analytical model of the IPMSM and setup the model in ANSYS Maxwell for finite-element analysis (FEA). In Section II-A, the basic analytical model of IPMSM is introduced, and in Section II-B, the 2-D model built in ANSYS Maxwell is presented.

A. Analytical Model

The average electromagnetic torque for IPMSMs is well established as given in (1), which is a combination of the reaction torque and the reluctance torque [19]

$$T = \frac{3}{2} p(\lambda_{\mathrm{PM}} i_q + (L_d - L_q) i_d i_q). \tag{1}$$

The total resultant torque of IPMSM can be viewed as an average torque and a pulsating torque which causes the torque ripple. The pulsating torque is mainly caused by three sources. The first source is the filed harmonic torque due to the nonideal sinusoidal distribution of the flux density in the air gap. The second source is the cogging torque caused by the reluctance torque that exists between the permanent magnets and the stator teeth, and the third source is the reluctance torque generated by the inequality of the d-axis and q-axis inductances, which is indicated in the second term of (1) [13]. According to the above-mentioned analysis, the flux distribution can directly affect the quality of the total torque in the machine. It is, therefore, necessary to analyze the air-gap profile (the rotor surface shape in this case) so that an optimal design for the rotor with minimum pulsation can be obtained.

B. 2-D Model in ANSYS Maxwell

A 2-D model of a 1 hp, three phases, six poles IPMSM has been constructed in the ANSYS Maxwell to validate the proposed method using FEM. Fig. 1(a) and (b) shows the complete model and the rotor model of this motor. To reduce the simulation time and in view of the symmetry in the motor, only one pole needs to be simulated [shown in Fig. 1(c)]. Detailed parameters and dimensions of the motor are shown in Table I [20]. FEA simulations are executed at the rated operating point.

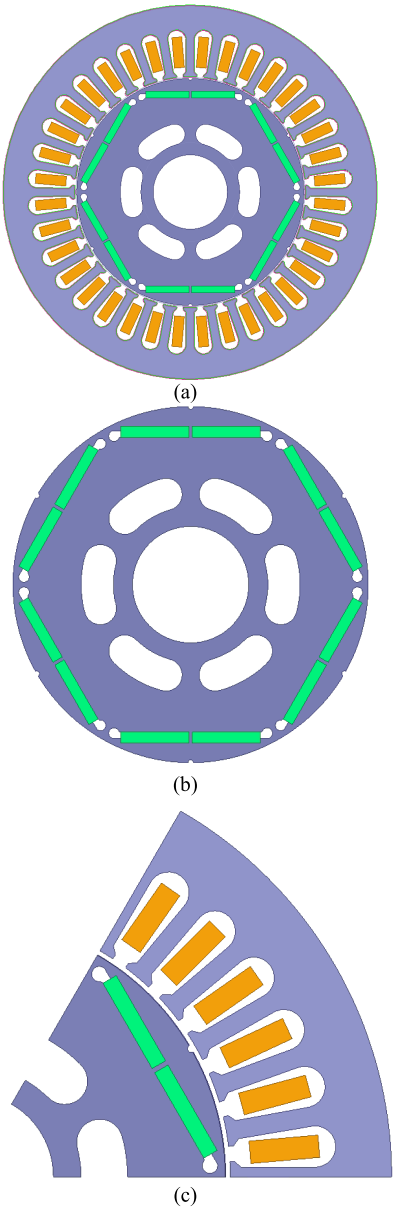

Fig. 1. (a) Complete IPMSM model. (b) Rotor model. (c) One pole pitch.

TABLE I
IPMSM Dimensions and Parameters [20]

Dimensions and Parameters	Quantity
Number of Poles	6
Number of Phases	3
Number of Slots	36
Rated Speed (rpm)	1800
Rated Power (hp)	1
Rated Torque (Nm)	3.9
Outer Diameter of Stator (mm)	139
Inner Diameter of Stator (mm)	85.85
Outer Diameter of Rotor (mm)	84.35
Air-gap (mm)	0.75
Stack Length (mm)	50.8

III. Grid On/Off Search Method

A. Grid On/Off Search Method

Air-gap profile heavily depends on the shape of rotor surface, which can cause a great difference in the distribution of flux and the forces acting on the rotor and stator through which torque performance would be influenced. The goal of torque ripple optimization is to redistribute the flux lines more

uniformly in the air gap and to reduce the bending at the interface of rotor and air gap due to slot openings on the stator. Therefore, it is very important to explore the rotor surface shape to optimize the air-gap profile in order to obtain an optimal design which provides the best torque performance.

To investigate the air-gap profile on reducing torque ripple, it is necessary to analyze the effects of slot opening on torque ripple since cogging torque is caused by the interaction between the magnetic field of permanent magnets and the stator slots depends strongly on the slot opening/slot pitch ratio [7]. It is important to note that in the presence of a slot-free stator and round rotor surface there are no cogging torque. Hence, if an equivalent air-gap length representing the impact of the slot opening can be found, it can be used as a step toward reducing/eliminating the cogging torque. To this end, one can note that the relationship between slot opening and air-gap length can be described by Carter's coefficient [21], [22] which determines an effective air-gap length to obtain the MMF across the air gap. This equivalent air-gap approximates the air gap of a slot-free stator which generates the same MMF as observed in the real stator. The Carter's coefficient for this motor is obtained by the following equation [23]:

$$C_S = \frac{w_{ss} + w_{st}}{w_{st} + \frac{4g}{\pi}\ln\left(1 + \frac{\pi w_{ss}}{4g}\right)} \tag{2}$$

where w_{ss} is the stator slot width (4.86 mm), w_{st} is the stator tooth width (2.49 mm), and g is the air-gap length (0.75 mm). The effective air-gap length g' is calculated according to the following equation [23], which is 0.9 mm:

$$g' = gC_S. \tag{3}$$

Applying the above-mentioned formulae to the machine under consideration will result in a difference of 0.15-mm layer on the rotor surface which leads to less cogging torque. In fact, if the surface of the rotor is sculptured according to the slot opening using Carter's coefficient one would expect to remove the cogging torque entirely. However, this computation would be valid for one rotor position and over a complete electrical cycle, various permutations of rotor surface are needed. Taking into account, the impact of commutation torque and its addition to torque pulsation one needs to perform an optimization through comprehensive numerical simulation to find an ideal surface profile. This has been the underlying principle of our optimization philosophy. Furthermore, due to manufacturing limitations, the precision is limited to 0.1 mm. Meanwhile, as air-gap length increasing, the average torque would be punished. In this case, the thickness of 0.1 mm of the grid on the rotor surface is selected.

In this paper, a layer of 20 partitions with a thickness of 0.1 mm and an angular span of 3° have been introduced to the rotor surface for each pole. The number of partitions is chosen according to the angle of each pole (60°) such that each partition has an integer angle. Simulation time also restricts the number of partitions since the number of all the combinations presents an exponential growth according to the number of partitions, too many partitions would consume much more time.

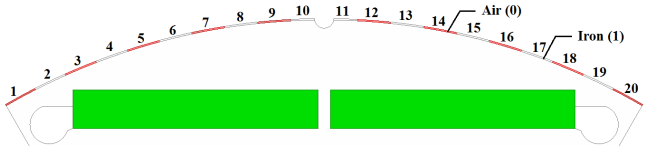

Fig. 2. Sample rotor profile with a hybrid combination of the air and iron partitions.

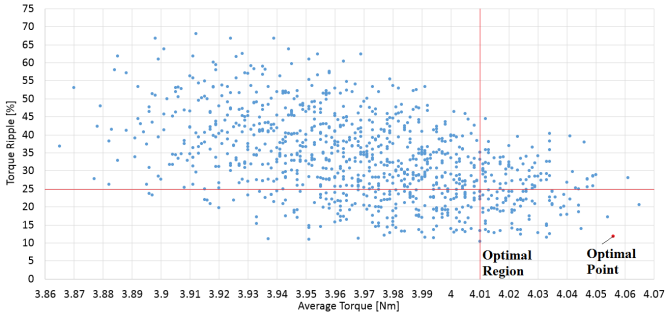

Fig. 3. Average torque versus torque ripple.

In each iteration, 20 partitions can be combined with different permutations of air and iron. Thanks to symmetry, the layout of 20 partitions is symmetric for each pole, so that all the possible permutations for only ten partitions for half of a pole are simulated in Maxwell at the rated operating point. A sample rotor profile with a hybrid combination of the air and iron is shown in Fig. 2 as an example. The material of each partition can be assigned as either air or iron, represented as "0" and "1" (shown in red and white in Fig. 2, respectively.). Fig. 3 illustrates the average torque versus torque ripple plot, and notably, an optimal region can be distinguished in which the lowest torque ripple and higher average torque are achieved.

B. Genetic Algorithm

In order to reduce simulation time as well as the engineering effort, the GA toolbox in MATLAB has been used to assist with the optimization method. This combination helps to find the global minimum for the targeted objective function.

MATLAB has been coupled with ANSYS Maxwell through the Visual Basic Script exported from Maxwell to automate the simulation process. In each iteration, MATLAB command controls Maxwell to execute the simulation, and the torque information is exported in Excel files and loaded into MATLAB. GA analyzes the data and decides if it gives the desired minimum value, if it does, the simulation terminates, and the minimum value as well as the optimal design variables will be recorded. Otherwise, GA will provide a new group of design variables for the combination of "0"s and "1"s for ten partitions and rewrite them in the script to execute another iteration of the Maxwell simulation until it finds the global minimum. Population size, maximum number of generations, and chromosome length are set to 100, 10, and 10, respectively. The flowchart in Fig. 4 shows the overall optimization process.

The objective function, in this case, is to minimize the torque ripple and to maintain or exceed the average torque

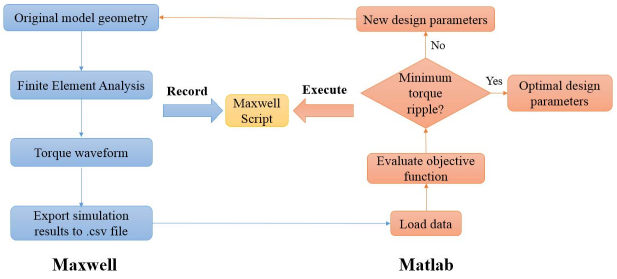

Fig. 4. Overall design optimization flowchart.

with respect to the original design. As GA always searches for the minimum value, the objective function is defined as

$$F = K_1 \left(\frac{T_{\max} - T_{\min}}{T_{\text{avg}}} \right) + K_2 \frac{1}{T_{\text{avg}}} \tag{4}$$

where $T_{\max}$, $T_{\min}$, and T_{avg} are the maximum, minimum, and average torque, respectively. K_1 and K_2 are the weights for torque ripple and the reciprocal of average torque, depending on which part is more important for the optimization due to application requirements. Since minimizing torque ripple and maximizing average torque are equally important in this case, K_1 and K_2 both are set to 0.5. The input variable, shown in (5), is a vector (i.e., chromosome) of the possible materials for ten partitions, which is either air or iron represented as "0"s and "1"s

$$X = [X_1 \quad X_2 \quad \ldots \quad X_{10}]. \tag{5}$$

IV. Simulation Results

The optimal design of the rotor surface is obtained and the input variable of the optimal design detected by the proposed method is given as

$$X = [0 \quad 0 \quad 0 \quad 0 \quad 1 \quad 1 \quad 1 \quad 1 \quad 1 \quad 0]. \tag{6}$$

Comparison of the original and the optimal designs of the rotor surface is shown in Fig. 5. It must be noted that structure dimensions such as the outer diameter and inner diameter of the stator, the outer diameter of the rotor, the minimum air-gap length, and the stack length for original and optimal designs are all the same. The only difference between these two designs is the fact that the original rotor surface is smooth and has a constant radius, while the optimal rotor results in an unequal air-gap length. The depth of carved areas is 0.1 mm.

Complete study including the torque performances, flux densities in the stator and air gap, the tangential and radial forces acting on the rotor surface and the stator teeth, as well as the structural analysis has been done for both of the original and optimal designs to verify the feasibility of the proposed method as well as the optimal structure. All the simulation results are obtained at the rated operating point shown in Table I. Three-phase sinusoidal currents with 1.2-A root-mean-square value and 120° phase shift are applied to excite the machine for both of the original and optimal designs.

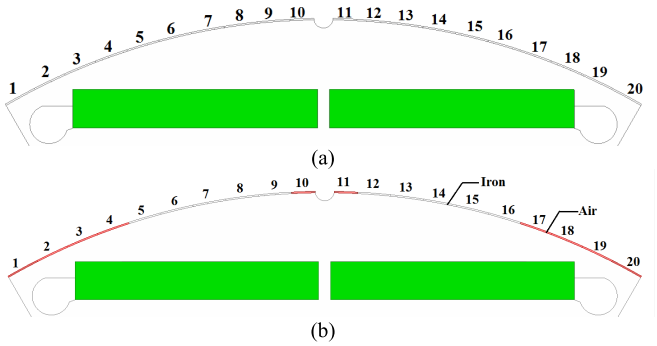

Fig. 5. (a) Original and (b) optimal rotor designs.

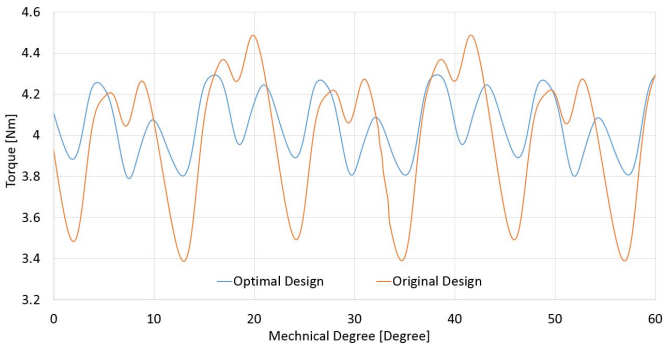

Fig. 6. Comparison of the original and the optimal torque waveforms.

TABLE II
Data Comparison of the Original and the Optimal Torque

	Original	Optimal	Comparison
Average Torque	4.01 Nm	4.05 Nm	1.12% ↑
Torque Ripple	27.56%	12.05%	56.27% ↓

A. Torque Performance Analysis

Fig. 6 shows the comparison of the torque waveforms of the original and the optimal designs. Torque ripple was significantly reduced from 27.56% to 12.05% which represents a 56.27% reduction. The average torque is increased from 4.01 to 4.05 N · m which indicates a 1.12% of increase. This comparison indicates that the grid on/off search method for the optimal air-gap profile is practical for torque pulsation mitigation. Not only the torque ripple is effectively reduced but also the average torque is slightly increased. The data comparison is concluded in Table II.

B. Flux Density in the Stator

Fig. 7 shows the flux density in one of the stator teeth according to the rotor position for one electrical cycle for both of the original and optimal designs. The highest point of the flux densities for both of the designs is around 1.78 T. Since the core material of rotor and stator is silicon steel M-15, no saturation occurs in either of the designs. It also expected that the core losses in both cases to be very similar.

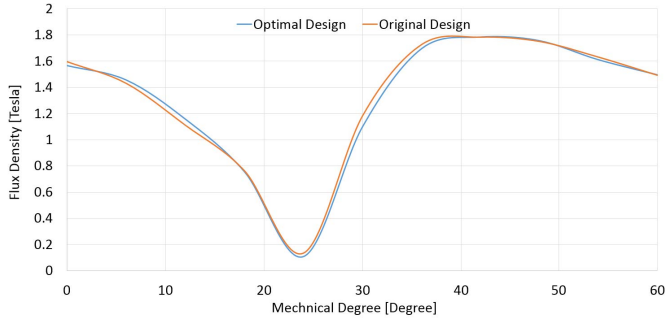

Fig. 7. Flux density in the stator teeth versus the rotor position for one pole.

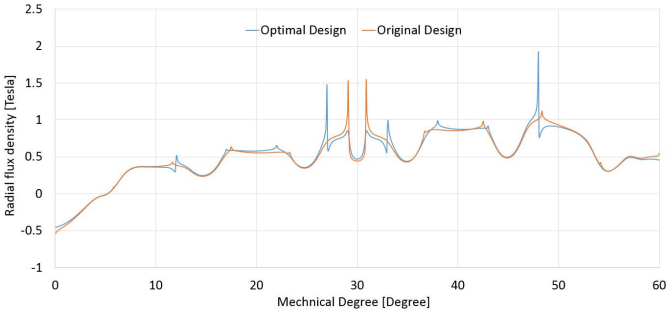

Fig. 8. Radial flux densities in air gap for original and optimal designs.

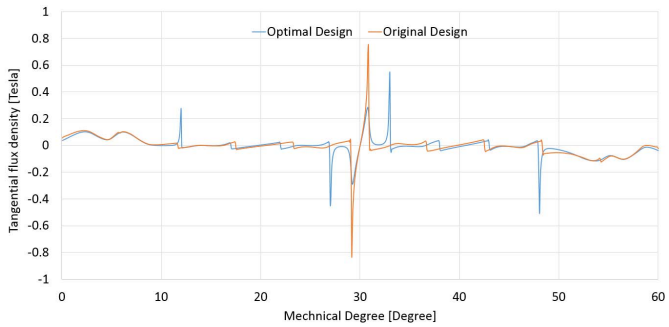

Fig. 9. Tangential flux densities in air gap for original and optimal designs.

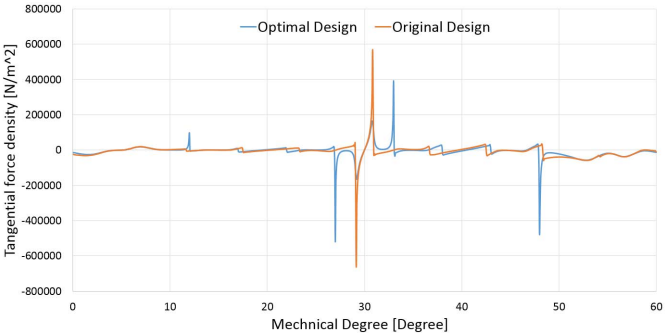

Fig. 10. Tangential force densities for original and optimal designs.

C. Flux Densities in the Air Gap and Tangential Force on the Rotor Surface

The tangential force acting on the rotor surface has been analyzed. These forces contribute to the torque production and are desired to be larger. The normal and tangential flux densities B_{n} and B_{t} are calculated in Maxwell which are shown in Figs. 8 and 9, respectively, can be used to calculate the tangential force density using Maxwell stress tensor [24], [25]

$$f_t(\theta_r) = \frac{B_{\mathrm{n}}(\theta_{\mathrm{r}})B_{\mathrm{t}}(\theta_{\mathrm{r}})}{\mu_0} \tag{7}$$

where μ_0 is the air permeability constant, and θ_{r} is the position of the rotor surface, θ_{r} spans over a range of 60° for each pole. Fig. 10 shows the tangential force densities on the rotor surface for both original and optimal designs for each pole. The average tangential force density of the original design is 132.5 N/m^2 higher compared to the optimal design, which contributes to a higher average torque. Total torque can be calculated using the following equation [25]:

$$T_e = 6\sum_{\theta_{\mathrm{r}}=0}^{60} \frac{1}{\mu_0} B_{\mathrm{n},\theta_{\mathrm{r}}} B_{\mathrm{t},\theta_{\mathrm{r}}} r^2 l \,\Delta\theta_{\mathrm{r}} \tag{8}$$

where $B_{\mathrm{n},\theta_{\mathrm{r}}}$ and $B_{\mathrm{t},\theta_{\mathrm{r}}}$ are the radial and tangential flux densities on the rotor surface at certain angle θ_{r}, r is the rotor radius, and l is the total stack length. The calculated average torque for original and optimal designs is 4.08 and 4.15 N · m, both of the results are slightly higher than the simulation results, which is due to the difference of the FEM and the Maxwell stress tensor. However, both results indicate that the optimal design provides higher average torque than the original design.

V. Structural Analysis

It is important to check if the optimal design is structurally reliable. The static structural analysis in ANSYS Workbench has been performed on the stator by applying the calculated radial forces on the surfaces of the stator teeth in order to explore the total deformation and the equivalent stress caused by the vibration for both designs.

A. Radial Forces Acting on the Stator Teeth

Radial forces acting on the stator teeth are the main source of the vibration in the stator which contributes to acoustic noise [26]. The radial forces on the stator teeth can be calculated according to the following equation [24], [25]:

$$f_r(\theta_{\mathrm{s}}) = \frac{B_{\mathrm{n}}(\theta_{\mathrm{s}})^2 - B_{\mathrm{t}}(\theta_{\mathrm{s}})^2}{2\mu_0} \tag{9}$$

where θ_{s} is the position angle on the surface of the stator teeth. Fig. 11 shows the radial force density acting on the stator teeth versus the mechanical degree of the stator teeth and slots for one pole. The optimal design has slightly lower magnitude than the original design such that radial forces acting on the stator for the optimal design are less, and the vibration as well as the acoustic noise will be smaller compared to the original design.

B. Structural Analysis

Forces acting on each stator tooth can be calculated by integrating the force density on the stator teeth surface. The calculated forces for six teeth of each pole for both the original and optimal designs at rated operating point are listed

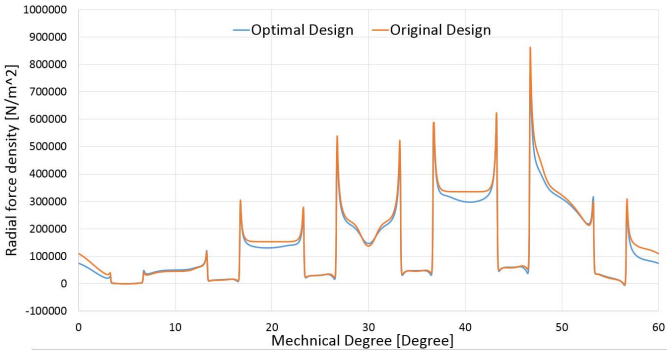

Fig. 11. Radial force densities for original and optimal designs.

TABLE III
RADIAL FORCES ACTING ON STATOR TEETH

Stator tooth	Radial force (Original design)	Radial force (Optimal design)
1	533.4 N	380.1 N
2	247.5 N	265.4 N
3	829.5 N	741.2 N
4	1178.8 N	1131.3 N
5	1816.7 N	1691.0 N
6	1767.2 N	1676.5 N

in Table III. The radial forces are calculated according to the radial force densities obtained from the Maxwell stress tensor, it is shown in Fig. 11 that the radial force density of the second stator tooth of the optimal design is slightly higher than the original design, which causes a higher radial force acting on the stator teeth. Since the optimization goal is to reduce torque ripple and to increase average torque, structural analysis is mainly for verifying the superiority and the feasibility of the proposed design, it is possible that one of the stator teeth has higher radial force than the original design. However, the overall performance of the optimal design is improved. Due to the symmetry, these forces can be applied to the stator teeth surface for all of the six poles under the rated operating point in the structural analysis.

Fig. 12 shows the total deformation and equivalent stress of the stator under the applied radial forces on the stator teeth for the original design. In this case, the maximum deformation is 0.008 mm, which is within the safe range as it is very small compared to the 0.75-mm air-gap length. The maximum equivalent stress is 28.7 MPa, which is within the safe range as the tensile yield strength for electric steel is about 358 MPa [27]. Fig. 13 shows the same plots for the optimal design, the maximum value of the total deformation is decreased by 6.25%, which is 0.0075 mm, and the maximum value of the equivalent stress is also decreased by 7.32%, which is 26.6 MPa. Both of the deformation and stress are reduced in optimal design.

The structural analysis results indicate that the optimal design obtained by the proposed method not only reduced the torque pulsation and increased the average torque but also reduced the radial forces acting on the stator teeth. In summary, it shows that the optimal design has better structural performance than the original design.

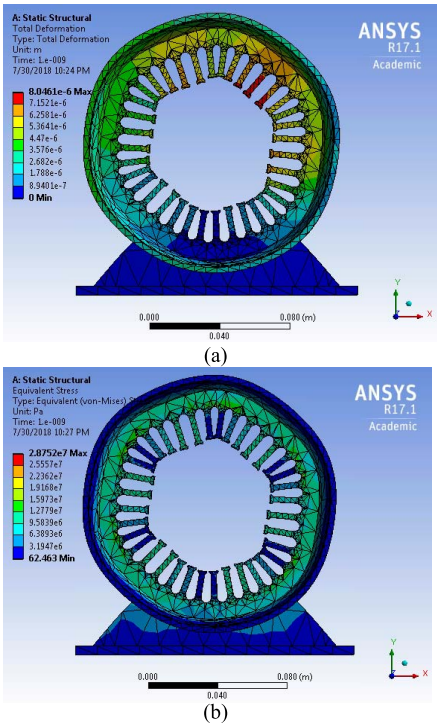

(a)

(b)

Fig. 12. Structural analysis for the original model. (a) Total deformation. (b) Equivalent stress.

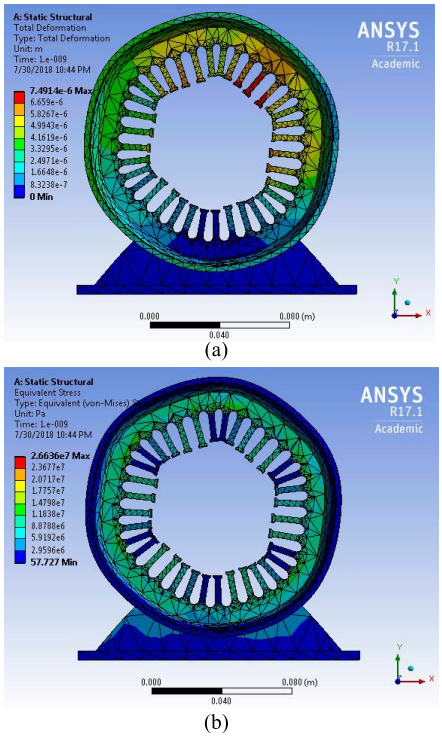

(a)

(b)

Fig. 13. Structural analysis for the optimal model. (a) Total deformation. (b) Equivalent stress.

C. Comparison With Similar Techniques

Results of the proposed optimal design have been compared with an inverse cosine with optimal third harmonic shaped rotor reported in [15] for torque ripple minimization.

TABLE IV
COMPARISON WITH SIMILAR TECHNIQUE

Parameters changes	Proposed optimal design	Inverse cosine shaped with optimal 3rd harmonic
Rated speed (rpm)	1800	400
Air-gap length (mm)	0.75	0.5
Torque ripple	56.27% ↓	59.42%↓
Average torque	1.12% ↑	5.11%↓

Both techniques have significantly reduced torque ripples compared to their original designs. However, the inverse cosine with optimal third harmonic shaped rotor has also punished the average torque by 5.11%. Detailed comparisons are presented in Table IV. In addition, the proposed optimal design is very easy to be manufactured compared to other techniques since it can be accomplished by laser cutting which would not cause any extra cost.

VI. CONCLUSION

In this paper, a grid on/off search method optimization of the air-gap profile is proposed for mitigating the torque pulsation of an IPMSM motor. GA has been applied to this method to further reduce the simulation time. The FEM simulation results indicate that the optimal design reduces torque pulsation by 56.27% and increases average torque by 1.12%. Radial forces acting on the stator teeth are also reduced in the optimal design, thereby causing a reduction of the total deformation and the equivalent stress according to the structural analysis. This optimal rotor design is easily applicable in the manufacturing process compared to other rotor shape optimization methods.

REFERENCES

[1] I. Boldea and L. N. Tutelea, *Electric Machines: Steady State, Transients, and Design With MATLAB*. Boca Raton, FL, USA: CRC Press, 2009.

[2] A. Emadi, *Energy-Efficient Electric Motors*, 3rd ed. Boca Raton, FL, USA: CRC Press, 2004.

[3] W. Wang, B. Fahimi, and M. Kiani, "Maximum torque per ampere control of permanent magnet synchronous machines," in *Proc. 20th Int. Conf. Elect. Mach.*, Marseille, France, Sep. 2012, pp. 1013–1020.

[4] L. Guo and L. Parsa, "Torque ripple reduction of the modular interior permanent magnet machines using optimum current profiling technique," in *Proc. IEEE IEMDC*, May 2009, pp. 1094–1099.

[5] G.-H. Lee, S.-I. Kim, J.-P. Hong, and J.-H. Bahn, "Torque ripple reduction of interior permanent magnet synchronous motor using harmonic injected current," *IEEE Trans. Magn.*, vol. 44, no. 6, pp. 1582–1585, Jun. 2008.

[6] J. W. Jiang, B. Bilgin, Y. Yang, A. Sathyan, H. Dadkhah, and A. Emadi, "Rotor skew pattern design and optimisation for cogging torque reduction," *IET Electr. Syst. Transp.*, vol. 6, no. 2, pp. 126–135, Jun. 2016.

[7] R. Islam, I. Husain, A. Fardoun, and K. McLaughlin, "Permanent-magnet synchronous motor magnet designs with skewing for torque ripple and cogging torque reduction," *IEEE Ind. Appl.*, vol. 45, no. 1, pp. 152–160, Jan./Feb. 2009.

[8] H.-S. Chen, D. G. Dorrell, and M.-C. Tsai, "Design and operation of interior permanent-magnet motors with two axial segments and high rotor saliency," *IEEE Trans. Magn.*, vol. 46, no. 9, pp. 3664–3675, Sep. 2010.

[9] S.-H. Han, T. M. Jahns, and W. L. Soong, "Torque ripple reduction in interior permanent magnet synchronous machines using the principle of mutual harmonics exclusion," in *Proc. IEEE Ind. Appl. Annu. Meeting*, New Orleans, LA, USA, Sep. 2007, pp. 558–565.

[10] S. H. Han, T. M. Jahns, and Z. Q. Zhu, "Design tradeoffs between stator core loss and torque ripple in IPM machines," *IEEE Trans. Ind. Appl.*, vol. 46, no. 1, pp. 187–195, Jan. 2010.

[11] K.-C. Kim, "A novel method for minimization of cogging torque and torque ripple for interior permanent magnet synchronous motor," *IEEE Trans. Magn.*, vol. 50, no. 2, pp. 793–796, Feb. 2014.

[12] A. Kiyoumarsi and M. Moallem, "Optimal shape design of interior permanent-magnet synchronous motor," in *Proc. IEEE Int. Conf. Electr. Mach. Drives*, San Antonio, TX, USA, May 2005, pp. 642–648.

[13] A. Kioumarsi, M. Moallem, and B. Fahimi, "Mitigation of torque ripple in interior permanent magnet motors by optimal shape design," *IEEE Trans. Magn.*, vol. 42, no. 11, pp. 3706–3711, Nov. 2006.

[14] K.-Y. Yoon and B.-I. Kwon, "Optimal design of a new interior permanent magnet motor using a flared-shape arrangement of ferrite magnets," *IEEE Trans. Magn.*, vol. 52, no. 7, Jul. 2016, Art. no. 8106504.

[15] K. Wang, Z. Q. Zhu, G. Ombach, and W. Chlebosz, "Optimal rotor shape with third harmonic for maximizing torque and minimizing torque ripple in IPM motors," in *Proc. Int. Conf. Elect. Mach.*, Marseille, France, Sep. 2012, pp. 397–403.

[16] S. Chaithongsuk, N. Takorabet, B. Nahid-Mobarakeh, and F. Meibody-Tabar, "Optimal design of PM motors for quasi-sinusoidal air-gap flux density," in *Proc. 45th Int. Univ. Power Eng. Conf. (UPEC)*, Cardiff, U.K., Aug./Sep. 2010, pp. 1–6.

[17] S. A. Evans, "Salient pole shoe shapes of interior permanent magnet synchronous machines," in *Proc. 19th Int. Conf. Elect. Mach. (ICEM)*, Rome, Italy, Sep. 2010, pp. 1–6.

[18] U.-J. Seo, Y.-D. Chun, J.-H. Choi, P.-W. Han, D.-H. Koo, and J. Lee, "A technique of torque ripple reduction in interior permanent magnet synchronous motor," *IEEE Trans. Magn.*, vol. 47, no. 10, pp. 3240–3243, Oct. 2011.

[19] S. T. Lee and L. M. Tolbert, "Analytical method of torque calculation for interior permanent magnet synchronous machines," in *Proc. IEEE Energy Convers. Congr. Expo.*, San Jose, CA, USA, Sep. 2009, pp. 173–177.

[20] L. Gu, "Modeling of permanent magnet machines using field reconstruction method," Ph.D dissertation, Dept. Elect. Comput. Eng., Univ. Texas Dallas, Richardson, TX, USA, 2016. Accessed: Dec. 2016. [Online]. Available: http://libtreasures.utdallas.edu/xmlui/handle/10735.1/5194

[21] F. W. Carter, "The magnetic field of the dynamo-electric machine," *J. Inst. Elect. Eng.*, vol. 64, no. 359, pp. 1115–1138, 1926.

[22] O. Laldin, S. D. Sudhoff, and S. Pekarek, "Modified Carter's coefficient," *IEEE Trans. Energy Convers.*, vol. 30, no. 3, pp. 1133–1134, Sep. 2015.

[23] P. Krause, O. Wasynczuk, S. D. Sudhoff, and S. Pekarek, *Analysis of Electric Machinery and Drive Systems*, 3rd ed. Piscataway, NJ, USA: IEEE Press, 2013.

[24] M. Kanematsu *et al.*, "Radial force control of IPMSM considering fundamental magnetic flux distribution," *IEEJ J. Ind. Appl.*, vol. 3, no. 4, pp. 328–334, 2014.

[25] W. Zhu, S. Pekarek, B. Fahimi, and B. J. Deken, "Investigation of force generation in a permanent magnet synchronous machine," *IEEE Trans. Energy Convers.*, vol. 22, no. 3, pp. 557–565, Sep. 2007.

[26] M. Krishnamurthy and B. Fahimi, "Qualitative analysis of force distribution in a 3-phase permanent magnet synchronous machine," in *Proc. IEEE Int. Electr. Mach. Drives Conf.*, Miami, FL, USA, May 2009, pp. 1105–1112.

[27] L. Maharjan, S. Wang, A. H. Isfahani, W. Wang, and B. Fahimi, "Comparative study of structural rigidity of induction machine and switched reluctance machine," in *Proc. IEEE Transp. Electrific. Conf. Expo (ITEC)*, Dearborn, MI, USA, Jun. 2014, pp. 1–5.

Jingchen Liang (S'17) received the B.S. degree in detection guidance and control technology from Northwestern Polytechnical University, Xi'an, China, in 2014, and the M.S. degree in electrical engineering from The University of Texas at Dallas, Richardson, TX, USA, in 2016, where she is currently pursuing the Ph.D. degree.

In 2016, she joined the Renewable Energy and Vehicular Technology Laboratory, The University of Texas at Dallas. Her current research interests include design, modeling, and control of electric machines and motor drives.

Amir Parsapour received the B.Sc. degree in electrical engineering from the Isfahan University of Technology, Isfahan, Iran, in 2005, and the M.Sc. and Ph.D. degrees in electrical engineering from the University of Isfahan, Isfahan, in 2009 and 2015, respectively.

His current research interests include design, modeling, and control of electric machines and intelligent system application in control and estimation.

Zhuo Yang (S'17) received the B.Sc. degree in electrical engineering from Wuhan University, Wuhan, China, in 2012, the M.Sc. degree in electrical engineering from the University of Florida, Gainesville, FL, USA, in 2014, and the Ph.D. degree in electrical engineering from The University of Texas at Dallas, Richardson, TX, USA, in 2018.

In 2015, he joined the Renewable Energy and Vehicular Technology Laboratory, The University of Texas at Dallas. His current research interests include renewable energy systems and energy storage systems.

Carlos Caicedo-Narvaez (S'16) received the B.Sc. degree in electrical engineering from The University of Texas at Dallas, Richardson, TX, USA, in 2014, where he is currently pursuing the Ph.D. degree in power electronics and energy systems.

He is currently a Researcher and Thrust-Area Leader (motors and motor drives) with the Renewable Energy and Vehicular Technology Laboratory, The University of Texas at Dallas. His current research interests include health diagnostics of electric machines, power electronics applications for Internet of Things, firmware implementation, and systems integration.

Mehdi Moallem (SM'90) received the Ph.D. degree in electrical engineering from Purdue University, West Lafayette, IN, USA, in 1989.

He is currently a Full Professor with the Department of Electrical and Computer Engineering, Isfahan University of Technology, Isfahan, Iran. He has authored or co-authored various journal and conference papers. His current research interests include design and optimization of electromagnetic devices, application of advance numerical techniques and expert systems to analysis and design of electrical machines, and power quality.

Babak Fahimi (S'96–M'99–SM'03–F'15) received the B.S. and M.S. degrees (Hons.) in electrical engineering from the University of Tehran, Tehran, Iran, in 1991 and 1993, respectively, and the Ph.D. degree in electrical engineering from Texas A&M University, College Station, TX, USA, in 1999.

He is currently a Distinguished Chair of engineering and the Founding Director of renewable energy and vehicular technology with The University of Texas at Dallas, Richardson, TX, USA. He has authored or co-authored over 330 scientific articles, 15 book chapters, and several technical reports in the general area of adjustable speed motor drives and power electronics. He holds 19 U.S. patents and has six more pending. He has supervised 26 Ph.D. (five tenured/tenure track professors) and 20 M.S. students.

Dr. Fahimi is a fellow of IEEE for his contributions to modeling and analysis of adjustable speed ac motor drives. He was a recipient of the DAAD Scholarship from 1993 to 1995, the IEEE R.M. Bass Power Electronics Young Investigator Award in 2003, the SAE Ralph Teetor Educational Award in 2008, the Fulbright Scholarship in 2010, and the IEEE Cyril Veinott Electromechanical Energy Conversion Award in 2015.